Journal of Electric Propulsion

RESEARCH Open Access

# Aromatic hydrocarbons as Molecular Propellants for Electric Propulsion Thrusters

André Nyberg Borrfors[1,2], Dan J. Harding[3], Jonas Weissenrieder[4], Simone Ciaralli[5], Ashley Hallock[5] and Tore Brinck[1*]

*Correspondence:
tore@kth.se

[1] Department of Chemistry, KTH Royal Institute of Technology, Stockholm SE 100 44, Sweden
[2] Present Address: Department of Chemistry, UZH University of Zürich, Zürich, Switzerland
[3] Department of Chemical Engineering, KTH Royal Institute of Technology, Stockholm SE 100 44, Sweden
[4] KTH, Materials and Nano Physics, Hannes Alfvens väg 12, Stockholm 11419, Sweden
[5] OHB Sweden AB, Viderögatan 6, Kista 164 29, Sweden

## Abstract

The aromatic hydrocarbons (AHs) fluorobenzene, naphthalene, and 1-fluoronaphthalene are introduced as promising alternatives to xenon as propellant for in-space electric propulsion (EP). These storable molecules have similar mass, lower cost, and lower ionization energies compared to xenon, as well as the critical advantage of low post-ionization fragmentation compared to other molecular propellant candidates. The ionization characteristics of AHs are compared with those of xenon and the diamondoid adamantane, previously evaluated as a molecular propellant for EP. Quantum chemical calculations and BEB theory together with 25 eV electron ionization mass spectrometry (EI-MS) measurements have been used to predict the fragmentation of the AHs and adamantane when ionized in a plasma with an electron temperature of 7 eV (a typical electron temperature in EP plasmas). A high fraction (81 – 86%) of the detected AH ions originate from intact molecules, compared to 34% for adamantane, indicating extraordinarily low fragmentation for the selected AHs. The ionization potential of the AHs is similar to that of adamantane but lower compared to xenon (8.14–9.2 eV for the AHs, 9.25 for adamantane and 12.13 eV for xenon). BEB calculations have also been used to predict total ionization cross sections. The calculated ionization cross section of the AHs is comparable to that of adamantane but 3–5 times higher than that of xenon, which together with the low ionization potential can contribute to more efficient ionization. The AHs may have the potential to perform better than xenon, despite the absence of fragmentation in xenon.

**Keywords:** Ionization cross section, Electron impact mass spectrometry, Ion thruster, Quantum chemical modeling, Ion fragmentation, Plasma modeling

## Introduction

Electric propulsion devices transfer momentum to a spacecraft by ionizing a propellant and electrically accelerating the resulting plasma to exhaust velocities an order of magnitude greater than what can be achieved with conventional chemical thrusters, allowing delivery of a higher delta-v compared to chemical propulsion for the same propellant mass. With the commercialization of space and the steadily increasing demand for affordable satellites, the market for more efficient and cost-effective electric propulsion thrusters has grown. Xenon has historically been the most common propellant for

electric propulsion subsystems, but has begun to be replaced with more affordable and more readily available alternatives such as krypton. A storable alternative to xenon offers advantages on subsystem level by eliminating the need for high-pressure propellant storage. In recent years the use of storable atomic propellants like bismuth and mercury for high thrust applications, and zinc and magnesium for high specific impulse applications has been investigated [1–4]. Some molecular propellants have been investigated, such as water (where the thruster operates on hydrogen and oxygen gas created by electrolysis) [5, 6], iodine [7–13], and adamantane [14–16], but were all found to have prohibitive disadvantages such as significantly lower performance compared to xenon. A paper on the first in-space demonstration of (low-power) thruster operation on iodine vapor was recently published in Nature [10]. Iodine offers a high storage density and vapor pressure combined with low ionization energy; however its reactivity introduces major challenges to development and implementation, especially for thrusters operating above 100 kW. The goal of this work is to identify and evaluate potential storable alternative EP propellants that have a mass and ionization efficiency comparable to that of xenon.

#### Ionization Properties of Molecular Propellants

The hydrocarbon molecule adamantane has previously been explored as a propellant for use in electric propulsion thruster [14–16]. Adamantane is the smallest diamondoid and has a mass similar to the xenon atom. Its ionization cross section is five times larger than that of xenon and its ionization energy (IE) is 9.25 eV compared to 12.13 eV for xenon [17]. It can serve as a scaffold for further molecular design and it is easily modified with a wide range of possible substituents; however experiments involving thruster operation on adamantane and a few of its substituted derivatives show fragmentation levels too high for these molecules to be effectively used as propellants for electric propulsion [15, 16].

In this study we propose aromatic hydrocarbons (AH) for use as molecular propellants as an alternative to xenon. In particular, we highlight the advantages of the hydro- and fluorocarbons fluorobenzene, naphthalene, and 1-fluoronaphthalene (Fig. 1). The availability of AHs (especially the smaller variants) is reflected in their low prices as is evident from Table 1 of Appendix A. While these are estimates and based on what was available from resellers at the time of asking, the AHs are generally around 10–100 times less expensive than xenon and much easier to procure.

These candidates were selected from a set of 13 different AHs (see Table 1 of Appendix A) by screening for desirable properties like high vapor pressure, appropriate

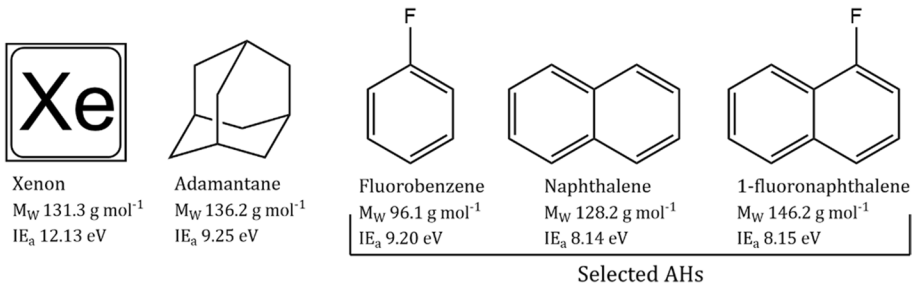


**Fig. 1** Molar mass and (adiabatic) ionization energies of adamantane and the AHs considered for use as molecular propellants in electric plasma thrusters

phase change temperatures, and low fragmentation during ionization as measured using standard electron ionization mass spectrometry. An inherent energy sink associated with ionizing molecules is the occurrence of fragmentation wherein some molecular ions break apart into multiple fragments where only one fragment remains charged. The additional energy of having to ionize any resulting neutral fragments can quickly compound because fragments are typically less stable than the original molecule and can dissociate even further. Therefore, molecular propellants that are stable both before and after ionization could offer a higher ionization efficiency compared to molecules with higher rates of fragmentation.

Compared to other molecules, AHs are unique in their stability towards ionization-induced dissociation because of their unique electronic and nuclear structures. In an AH, the electronic structure consists of a combination of σ- and π-orbitals, which provides additional stabilization upon ionization compared to saturated hydrocarbons such as adamantane. The σ-orbitals can be divided into lower-energy core orbitals and bonding valence orbitals. The latter make up a skeleton of single bonds between all atoms in the molecule. The π-orbitals are generally higher in energy and more delocalized in character, and together they contribute a partial double bond character to the bonds between all atoms of the ring system. Because of their higher energies, ionization typically leads to expulsion of an electron from a π-orbital, and this only partially reduces bond orders between the ring atoms as the σ-orbital single-bond skeleton remains intact. In the more unlikely event of ionization from a σ-orbital, individual σ-bonds may be weakened, but due to the extra bond-stabilization from the π-orbitals this is not likely to lead to bond rupture. In a saturated hydrocarbon, such as adamantane, ionization occurs predominantly from the valence σ-orbitals, and this will inevitably weaken the σ-bond skeleton, and it is highly likely to lead to bond rupture and fragmentation. The higher stabilities upon ionization of AHs compared to saturated hydrocarbons can be verified by comparing their electron ionization mass spectra (EI-MS), which show significantly higher fragmentation for the saturated hydrocarbons. It should be noted that low-fragmentation in EI-MS is not a sufficient criterium for a molecular propellant, as the $C_{60}$ molecule has performed poorly when tested in electric propulsion thrusters [18–20]. However, $C_{60}$ is not an aromatic molecule and despite the low fragmentation in EI-MS it is an inherently unstable and highly strained molecule [21], which together with its high sublimation enthalpy and its high propensity for electron attachment are believed to be the main reasons behind its poor performance [18–20]. None of these reasons apply to the AHs of this study.

AHs also possess remarkable resistance towards thermal degradation [22–25], with gas phase benzene and naphthalene starting to decompose in the range of 600–650 °C [26]. Heavier AHs than those in Fig. 1 consisting of an increasing number of fused carbon rings can also serve as viable propellant candidates and have even higher decomposition temperature, but the vapor pressure is lower than that of their smaller counterparts. This can lead to higher required heater power to maintain the propellant as a gas in the propellant feed system and potential deposition of propellant from the thruster plume on spacecraft surfaces. Vapor pressure curves for many AHs can be found in Appendix A, Fig. 6.

The properties of AHs are readily modified by chemical functionalization, i.e. one or more of the hydrogens can be substituted for another atom or functional group. The substitution of a hydrogen for a heavier element typically reduces the resistance towards

ionization-induced fragmentation. The only obvious exception is fluorine substitution, which generally has a minor effect on the fragmentation as long as the number of substitutions is limited. This anomaly can be traced to the relatively low weight of the fluorine in combination with the relatively high strength of the C-F bond. Substituting one of the hydrogens in naphthalene with a single fluorine atom increases the molecular mass by 14% from 128.2 to 146.2 amu and the aggregation state changes from solid to liquid at ambient temperature. Depending on the position of the fluorine two different naphthalene isomers can be constructed, namely 1-fluoronaphthalene and 2-fluoronaphthalene. These have slightly different physical properties, e.g. melting point, but their ionization behaviors and mass spectra are similar. Considering the similarity of the two isomers, only 1-fluoronaphthalene is considered in this work together with the other AHs.

The ionization cross sections of molecules are generally larger than for atoms and therefore a shorter plasma ionizing region is sufficient to reach the required degree of ionization for a molecular propellant. The most important ionization process taking place in typical electric propulsion thrusters is (e,2e) electron ionization, where a single incident electron with kinetic energy $T$ collides with a target and results in the expulsion of a bound electron. This creates a positively charged radical cation, which can be accelerated by an electric field to produce thrust. If $T$ is lower than the IE of the target atom or molecule, no ionization can occur from a single collision. If multiple collisions between a target and electrons (or other molecules when the pressure is high) are allowed, as in an ionizing plasma, less energetic collisions can still accumulate enough energy in the target to ultimately lead to ionization.

The power to thrust efficiency is important for the viability of a thruster and depends largely on the efficiency of ionizing the propellant. All processes not contributing to ionization represent an energy sink and within a molecular plasma these are numerous and complex. However, similarly as indicated in the study of adamantane, it can be expected that dissociation reactions caused by low energy (e,2e) ionization, which causes AH fragmentation on the order of 10–20% of the ionized propellant, will be the instrumental factor influencing the thruster performance [15]. Thus investigating the (e,2e) process and the ionization induced dissociation has been the main focus of this work, but the relative influences of other processes on the ionization efficiency will be analyzed and discussed in Sect. 4.1.

In this article, we will describe the experimental and analytical method of investigation of the ionization behavior of the molecules in Fig. 1. Results and discussion of ionization cross section calculations for the AHs and adamantane are followed by results and discussion of measurements of the fragmentation of the AHs and adamantane, including a comparison of the estimated ionization efficiency of the AHs and that of xenon. The predicted performance of a thruster operating on AHs is then discussed, along with a discussion of accommodation, safety and environmental aspects. The article concludes with a summary of findings regarding the suitability of the AHs as an alternative EP thruster propellant.

## METHODOLOGY

### Method of calculation of Ionization Cross Section

All quantum chemical calculations were performed using the Gaussian 16 software suite [27]. Relaxed molecular geometries were obtained through structure optimization using the hybrid M06-2X functional and the 6-311 g(d,p) basis set. Vertical ionization energies (IE)

used for producing BEB cross sections (see Appendix B, Eqs. 3 and [28, 29]) were obtained using electron propagator theory (EPT) based on Hartree-Fock (HF) wavefunctions and the 6-311 + g(2df,2p) basis set. In the cases where relativistic effects had to be accounted for, such as for BEB calculations involving xenon and iodine, the Def2-TZVPP basis set with effective core-pseudopotentials was used. BEB theory is most sensitive to the accuracy of the IE ($B$ in Eq. 3) associated with the highest energy valence orbitals. Therefore, when used to calculate $t = T/B$ for valence orbitals, the value of $B$ was taken to be the more accurate IE obtained by applying the P3 propagator in EPT. As EPT often struggles to converge when the IE is too high, only values of $B < 20$ eV were obtained using P3. For the remaining orbitals, and in the rare instances when P3 failed to converge while below the threshold, the IE was, by applying Koopmans theorem, taken to be the negative of the orbital binding energy obtained at the HF level of theory. HF was also used in producing the value of the orbital kinetic energy $U$, and by extension its reduced form $u = U/B$.

#### Method of measurement of ionization-induced fragmentation

Mass spectra were collected using a Pfeiffer QMA 400 Quadrupole mass spectrometer (MS) equipped with a Faraday cup detector and mounted on a small vacuum chamber capable of reaching $1 \times 10^{-8}$ mbar base pressure. Software for controlling the MS and collecting spectroscopic data was QUADERA (build 4.62.004). The chamber pressure was measured using a Balzers IKR-020 Penning Vacuum Gauge placed out of the line of sight of the MS ionizer. The Penning pressure detector is a cold cathode ionization-type vacuum gauge that uses a high electron current with a non-discrete and complex energy distribution to ionize gases within the chamber. The reported pressure is linearly dependent on the resulting ion current, which, in turn, depends on the appropriate cross sections of the gases. For simple and common gases (e.g., $H_2$, $N_2$, Ar) at low pressures, the correction factor for determining the real chamber pressure is known, but this is not the case for the molecular analytes covered in this study.

Initially, spectra were collected using a residual gas analyzer MS of the type RGA200 from Stanford Research Systems and showed a strong bias towards low mass fragments. Later measurements (Figs. 4 and 5 and *EI-MS* in Fig. 7 in Appendix A) instead used the Pfeiffer QMA 400 instrument, where it was verified that the spectra captured at 70 eV were consistent with literature.

Analytes were purchased from SigmaAldrich ($\geq$ 99% purity) and used as received. In order to introduce them into the vacuum chamber they were loaded into a test tube connected to a 16 mm Pfeiffer CF flange which could be mounted to the inlet system of the chamber and sealed with a copper gasket. The inlet system was connected to an oil-sealed vacuum pump which provided initial degassing of the inlet and sample. A ball valve was used to disconnect the backing pump (which was kept operating to prevent backflow) after which the variable leak valve leading to the chamber was opened and used to adjust the chamber pressure. Before each MS measurement, any volatile atmospheric gases introduced into the chamber during sample loading were slowly evacuated by a turbopump until only a trace amount of water could be detected. To protect the thermionic filament from overheating when running the MS at low electron energies an emission current of 0.1 A was used for all measurements (one tenth of the standard setting). To compensate for the resulting loss in signal intensity the chamber pressure was allowed to reach up to $5 \times 10^{-6}$ mbar during measurements, as reported by the Penning

gauge. To reduce baseline noise the collection of each spectrum was cycled four times and averaged. Measurements at different electron energies were performed in quick succession to ensure the chamber pressure did not drift appreciably.

Gas Chromatography Mass Spectrometry (GCMS) measurements were performed using a Trace 130CG (Thermo Fisher, Wahtlam, MA, US). coupled to an ISQ TL MS (Thermo Fisher). and controlled with the Xcalibur software. A Thermo Scientific TraceGOLD MTG-SQC GC column with dimensions $15m \times 0.25mm \times 0.25\mu m$ was used. Samples were prepared in 100 ug/ml solutions of cyclohexane and injected with split injection.

The GC oven starting temperature 40 °C was held for 90 s before increasing to 200 °C at a rate of 20 °C /s, then increasing again to a final temperature of 240 °C with a rate of 50 °C /s and held for 180 s. The MS used 70 eV electron impact ionization.

## RESULTS AND DISCUSSION

### Ionization Cross Section calculation results and discussion

The ionization cross section (analogous to the ionization probability) and the ionization energy (IE) are important properties of a propellant to maximize the performance and energy efficiency of a plasma thruster [30]. The IE of AHs can easily be found in the literature and are collected in Table 1 of Appendix A, but experimental cross sections are only available for some atoms and for the simplest AHs, and we therefore refer to ab initio quantum chemical calculations instead. In Fig. 2 the total ionization cross section curves from (e,2e) ionization as calculated using Binary Encounter Bethe (BEB) theory are shown for a selection of relevant atomic and molecular species. Through experiment the total cross sections of the noble gases argon and xenon have been determined to 1.23–3.52 and 2.62–7.31 $Å^2$, respectively, when ionized by 70–75 eV electrons [31, 32]. Through BEB calculations we obtain 2.06 and 4.17 $Å^2$, respectively, which are within the range of the experimental values. More importantly, BEB has been shown to accurately predict cross sections of many low mass molecules, including a range of different hydro- and fluorocarbons [33–35]. BEB cross sections of aromatic ring systems similar to small AHs are also known to be in excellent agreement with experimental values [36].

A clear separation in the cross sections between the included atoms and molecules can be observed in Fig. 2, where the former all have a cross section maximum in the range of 2 to 5 $Å^2$. The maxima of the latter lie above 8 $Å^2$ and rapidly ascend in order of increasing number of atoms of each respective molecule, starting with molecular iodine. For instance, adamantane and the naphthalenes have over 5 times the cross section of xenon, which would lead them being ionized after a much shorter time spent in the plasma. The cross-section curves of both atomic and molecular iodine are included in Fig. 2, as a large fraction of molecular iodine dissociates upon being ionized and the resulting uncharged iodine atom has to be ionized to produce thrust. The length $L$ of the effective ionizing region of the plasma in a plasma thruster is proportional to the ionization cross section of a given propellant averaged over a Maxwellian velocity distribution [30] by

$$L \propto \langle \sigma v_e \rangle^{-1}$$

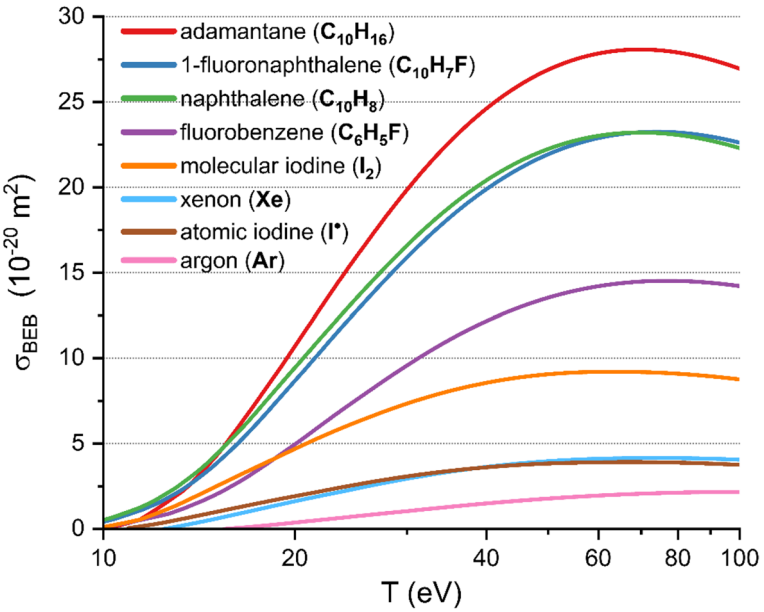


**Fig. 2** Total ionization cross sections calculated using BEB theory for the molecules in Fig. 1, argon, xenon, and atomic/molecular iodine. *T* is the kinetic energy of the incident electron impinging on the atom/molecule

Where $\langle \sigma v_e \rangle \approx \sigma(T_e)\overline{v}$ is the reaction rate coefficient that can be approximated by the product of the cross section averaged over a Maxwellian distribution of electrons with temperature $T_e$ and the average speed $\overline{v}$ of those electrons. Increasing L will increase the degree of ionization of the propellant fed to the thruster by allowing for more collisions with the plasma electrons and more energy transfer into the propellant. However, increasing energy deposited into the propellant leads to decreasing energy efficiency of the thruster, and in the case of a molecular plasma promotes molecular dissociation processes.

### Fragmentation Measurement results and discussion

Incident electrons of kinetic energy $T$ can cause ionization of the target atom or molecule through the (e,2e) mechanism, given that $T$ exceeds their respective vertical IE. Energy deposition resulting from successful (e,2e) collisions have been calculated based on BEB theory, and the gaussian-smoothed probability distributions (Eqs. 4–7, Appendix B) are displayed in Fig. 3 for adamantane and the selected AHs. By increasing $T$, more strongly bound electrons in the molecules become accessible and can participate in (e,2e), resulting in the noticeable decrease in relative intensity of the lowest energy peak for each molecule. This decrease is less pronounced for adamantane in Fig. 3 (A) compared with the AHs (BD) and should thus contribute to less variation in the degree of dissociation as $T$ increases. We will see later, however, that the proclivity of adamantane to undergo ionization induced dissociation is already very high at $T=25$ eV, and that the fragment abundance measured using standard 70 eV mass spectrometry is highly indicative of the stability (and lack thereof) at lower $T$.

In electrostatic EP thrusters ions created through collisions with energetic electrons are accelerated to high velocities to produce thrust. Due to the significant difference in mass between the electrons and the larger particles within the anode chamber, a heterogeneous plasma can be sustained where the ionized species are expelled before

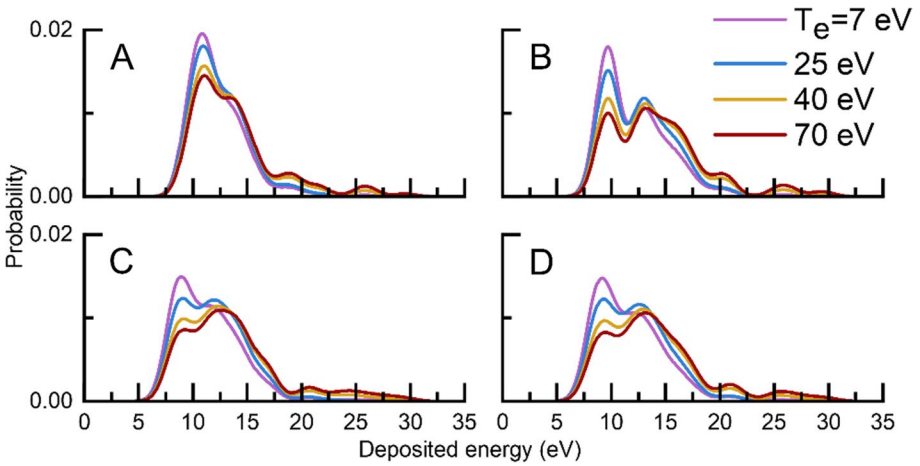


**Fig. 3** Computed probability distributions of the energy deposition caused by single collision (e,2e) ionization for the molecules (**A**) adamantane, (**B**) fluorobenzene, (**C**) naphthalene, (**D**) 1-fluoronaphthalene. The figure illustrates four (e,2e) scenarios: three where the incident electron kinetic energies $T$ range from 25 to 70 eV, and one where $T$ is dictated by a Maxwell-Boltzmann distribution of electron energies corresponding to a plasma temperature $T_e$ of 7 eV

thermal equilibrium with the electrons can be reached. The kinetic energy of the electrons in the ionizing plasma is here assumed to be well approximated by a Maxwell-Boltzmann distribution with a plasma temperature $T_e$=7 eV (see Appendix B, Eq. 6). This $T_e$ was selected to obtain results comparable with those reported by Dietz et al. in their study on plasma ionization of adamantane, xenon, and molecular iodine [15].

The calculated energy deposition caused by a Maxwellian plasma with an electron temperature $T_e = 7$ eV is also included for the molecules in Fig. 3 (purple curves). These curves are very similar, but slightly lower, to the (blue) curves resulting from (e,2e) with $T = 25$ eV. With the assumption of a low number of electron collisions taking place within the 7 eV plasma, the 25 eV (e,2e) measurement is well suited for estimating the adamantane fragmentation within such a plasma. This was verified in the current study where the 25 eV mass spectrum of adamantane agreed well with measurements made in the 7 eV plasma thruster by Dietz et al. (*vide infra*). Furthermore, the difference between energy deposition from low energy (e,2e) and plasma ionization for the selected AHs is more pronounced, indicating that electron energies even lower than $T = 25$ eV could be appropriate when simulating their behavior in a 7 eV plasma. Note that energy deposited into the propellant due to vibrational excitation is included in Fig. 3 as the BEB-calculations are using vertical ionization potentials as input. The importance of other processes than (e,2e) are not considered but their importance upon the ionization efficiency are discussed in Performance Predictions for AHs section.

The electron ionization mass spectra (EI-MS) of adamantane and the AHs can be seen in Fig. 4. The intensities observed in the measurements cannot be used to compare absolute ionization cross sections between the different analytes, as we had no reliable way of measuring the absolute pressure (see methods). However, the relative change in ion current as a function of $T$ for each analyte is easily determined and can be found in the right column of the tables in Fig. 4, as well as in Appendix A, Table 2. In Table 2 in Appendix A we also list the relative cross sections calculated using the BEB method. Immediately

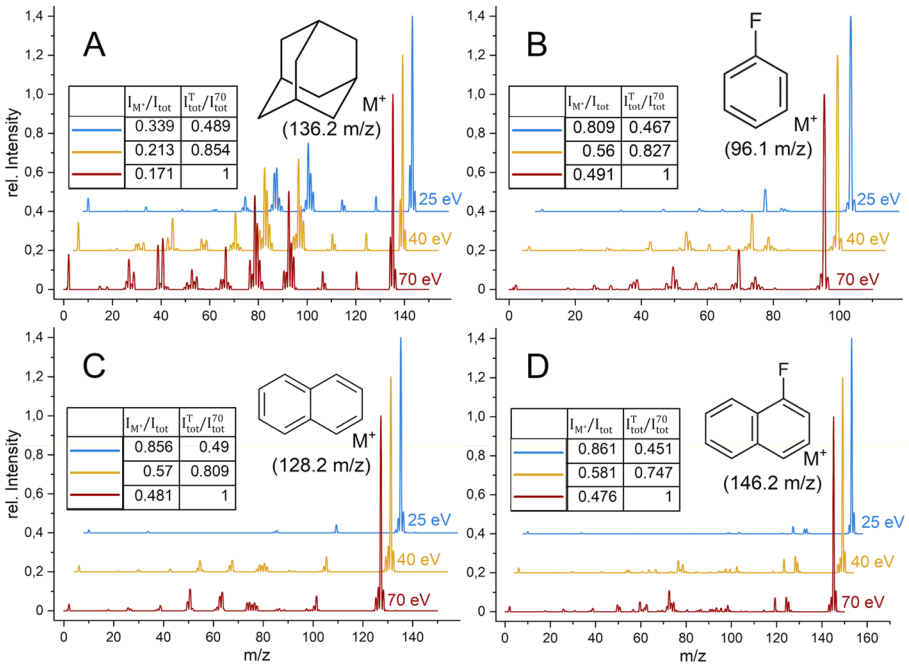


**Fig. 4** Mass spectra from the molecules (**A**) adamantane, (**B**) fluorobenzene, (**C**) naphthalene, (**D**) 1-fluoronaphthalene, collected at different incident electron energies T. The spectra collected at 40 and 25 eV have been horizontally offset by 4 and 8 m/z, respectively. For each molecule is included a table with the relative ion current of $M^+$ with respect to the total ion current $I_{M^+}/I_{tot}$ (left), and the relative total ion current with respect to the same total ion current measured at $I^T_{tot}/I^{70}_{tot}$ (right)

evident from the spectra is the much lower fragmentation of the AHs when compared with adamantane, and the similarly sized fragmentation peaks of the naphthalenes.

As mentioned earlier, adamantane has been shown to suffer from a high degree of fragmentation under conditions commonly found in EP thruster discharge chambers [14, 15]. Per Fig. 2; Table 2 (Appendix A), the BEB cross section of adamantane decreases by 12.3 and 43.1% when electron energy is reduced from 70 eV to 40 and 25 eV, respectively. This is reasonably well reflected by our measurements in Fig. 4 (A) by a 14.6 and 51.1% reduction, respectively. However, as can be seen in the low ratios in the left column of the table in (A), a very large part of the adamantane ion current stems from fragments of molecular dissociations. Even when using the low electron energy $T = 25$ eV only 33.9% of the signal is due to the adamantane molecular ion ($M^+$), a figure which rises to 41.3% (Table 2) in Appendix A if none of the neutral hydrogen loss from the parent molecule is counted towards fragmentation (i.e. $M^+ = [M\text{-}H_X]^+$ where $X \geq 0$). Each signal in Fig. 4 caused by the detection of an ionic fragment is associated with at least one additional neutral fragment which does not appear in the measured spectra. In a plasma thruster all such neutrals would have to be ionized before undergoing electric or electromagnetic acceleration, and for adamantane this would result in a very low energy efficiency because of the excessive fragmentation. The mass spectra measurements performed by Dietz et al. on the exhaust plume of a modified RIT thruster operating on adamantane (see Fig. 9 in [15]) show a very high abundance of fragments. The authors varied the mass flow of adamantane to the thruster as well as the power of the radio frequency generator (RFG) to estimate the effect of plasma temperature and electron-neutral collision

frequency on the molecular plasma composition. At the lowest RFG power, and with plasma temperature $T_e$ estimated to be $7 \pm 1$ eV, the relative abundance of $[M\text{-}H_X]^+$ ions exiting the RIT was roughly 36% of the total ion current. This high fragmentation agrees well with the value of 41.3% we obtained for $T = 25$ eV in the present work.

The behavior of the AHs in Fig. 4 under ionizing conditions is distinctly different from adamantane, whereas the differences between the individual AHs are rather small. We will therefore discuss the naphthalene spectra in more detail and compare them to the adamantane spectra. The mass spectra of naphthalene in Fig. 4 (C) display much less intense fragment ion signals in relation to $M^+$ for all $T$. Notably, naphthalene remains intact to a larger degree even at $T = 70$ eV ($I_{M+}$=48.1%) compared with adamantane at $T = 25$ eV ($I_{M+}$=33.9%). At 25 eV the percentage of intact naphthalene cations is 85.6% of the total ion current (92.5% for $[M\text{-}H_X]^+$), while the remaining 14.4% (7.5%) is due to detected fragment ions. The largest difference in fragmentation behavior is observed when $T$ is increased from 25 to 40 eV, which is consistent with the corresponding curves in Fig. 3 where the yellow and red lines (40 and 70 eV) overlap to a large extent. This highlights the importance of optimizing the ionization conditions of the plasma thruster to prevent excess energy being deposited into the propellant, as all fragmentation constitutes a loss of thruster efficiency. Combining the calculated cross sections in Fig. 2 with the relative ion current of the fragments, deduced from Fig. 4 by $I_{F+} = 1 - I_{M+}$ we can estimate semi-empirical electron impact dissociation cross sections for the AHs at the measured electron energies. These are (in $10^{-20}m^2$) for naphthalene 13.72 (70 eV), 8.78 (40 eV), 1.95 (25 eV); for fluoronaphthalene 12.17 (70 eV), 8.34 (40 eV), 1.78 (25 eV); and for fluorobenzene 7.37 (70 eV), 5.35 (40 eV), 1.44 (25 eV).

To increase legibility, the 25 eV mass spectrum of naphthalene was converted to a histogram bar graph by integrating the signals about each integer m/z. The result can be seen in Fig. 5 where the region 20–105 m/z has been scaled up and labels for the most abundant fragments have been included.

From Fig. 5 it is clear that for single collisions with low energy electrons, naphthalene is likely only to dissociate into a few select fragments. The rightmost peaks (m/z = 101, 102 amu) in the scaled-up figure, denoted $C_8H^+_{5-6}$, is the fragment associated with loss of acetylene, $C_2H_2$, whose signal is detected as the leftmost peak at m/z = 26 amu. Together, these constitute the full naphthalene molecule or in the case of any associated hydrogen loss, some version of $[MH_x]^+$. The remaining peak, $C_6H^+_{4-6}$, is associated with a fragment that appears with low intensity at m/z = 50 amu.

The situation becomes significantly more complex when a plasma is used for ionization. By colliding with energetic electrons, the energy of a molecule increases. If the pressure is high, this energy is rapidly distributed through molecule-molecule collisions, resulting in a rise in temperature. At higher temperatures, more dissociation pathways become available and, consequently, more unique fragments are created during ionization and can be detected from mass spectrometry. We performed high temperature gas chromatography mass spectrometry (GC-MS) at 250 °C and $T = 70$ eV electrons on the analytes in Fig. 4 (except fluorobenzene) to evaluate how their respective fragment abundances change when heated. The superimposed spectra from GCMS with those from relevant measurements in Fig. 4 can be found in Appendix A, Fig. 7. In the case of adamantane, GC-MS resulted in a noticeable increase in fragment intensities while the effect was more

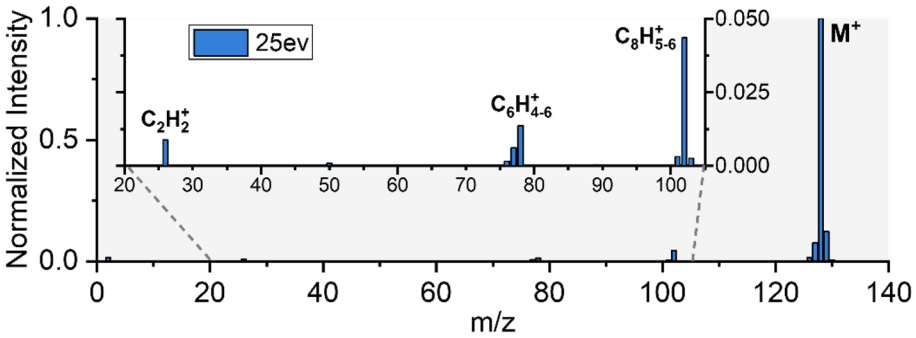


**Fig. 5** Histogram mass spectrum of naphthalene obtained at $T = 25$ eV incident electron energy, where the region 20–105 m/z has been scaled up

subdued for the naphthalenes, almost to the point of being indistinguishable when compared with the cold EI-MS experiment. Similar effects were reported by Eren et al. [37] who noted that "*… for small molecules (below 20 atoms) such as benzene ($C_6H_6$), no or very little vibrational cooling effect is observed in their Cold EI mass spectra, while compounds with 20–40 atoms show noticeable enhancement of their molecular ion abundance.*"

In a study by Alliati et al. [38] where they measured ionization of pure naphthalene vapor using a plasma sourced from a high-frequency RFG with power values in the range from 10- to 95 W, the types of fragments detected were almost identical to those we found when using T = 40 and 70 eV electrons in (e,2e) of naphthalene. The relative intensities of fragment peaks following plasma ionization were, however, found to be much lower and on par with our 25 eV measurements. The main difference is that the relative abundance of the acetylene $C_2H_2$ ion is also noticeably higher than what we find with EI-MS with $T_e$ =70 eV. This higher abundance of $C_2H_2^+$ can mainly be traced to the fragmentation of the naphthalene cation into $C_8H_6^+$ and neutral $C_2H_2$, as the latter is ionized in the plasma. The authors did not specify an electron temperature associated with the plasma electrons, or even if they could be considered Maxwellian and have a well-defined temperature, and therefore it is difficult to draw conclusions beyond these general observations in relation to the results obtained in this work. Nevertheless, their results are very encouraging and support our observations of naphthalene's stability under relevant conditions. It can further be noted that Najeeb and Kadhane performed EI-MS measurements with an electron temperature of 1 keV (1000 eV), and even at this very high temperature the naphthalene cation is the dominating species and the spectrum is remarkably similar to that at T = 70 eV [39]. The main difference is the appearance of a peak at m/z = 64 corresponding to doubly ionized naphthalene.

Expanding the discussion to include the rest of the AHs in Fig. 4, the relative ion current at $T = 25$ eV for naphthalene appears slightly higher than for 1fluoronaphthalene in accordance with the BEB cross sections in Fig. 2. Their fragmentation abundances are nearly identical at all $T$, confirming that the addition of a fluorine substituent has negligible effect on the molecular stability and that fluorine substitution is a useful tool which allows for expanding on the AHs capabilities as propellants. Fluorobenzene is slightly more prone to dissociate at $T = 25$ eV compared to the heavier naphthalenes, but the difference is minor and should not exclude fluorobenzene from being considered a viable propellant candidate.

Treating $[MH_X]^+$ ions as intact molecules despite loss of neutral hydrogen (as was done in the paper by Dietz et al. [15] when analyzing adamantane) increases the intact to total ion ratio of the $T = 25$ eV spectra from that of the right columns in Fig. 4 to 0.844, 0.925, and 0.897 for fluorobenzene, naphthalene, and 1-fluoronaphthalene, respectively. Disregarding hydrogen fragmentation is not entirely unwarranted, as both molecular and atomic hydrogen obtain considerable velocity when having undergone dissociation, due to their low mass. The ionization cross section of molecular hydrogen is around 0.5 $Å^2$ when T = 25 eV [40] and its 1st IE is over 15.4 eV, making it much less likely to be ionized by a plasma thruster designed and optimized for much heavier molecules with large cross sections and low IE. Atomic hydrogen even less so. One can speculate that hydrogen to some extent is expelled from the plasma as neutral species. In addition, atomic and molecular hydrogen are known to react with ionized AHs to form hydrogenated AH cations. These cations may expel hydrogen or dissociate into fragments but are most likely to remain intact until expulsion from the thruster [41]. Hydrogen abstraction is also known to promote the hydrogen-abstraction/acetylene-addition (HACA) mechanism [42]. Alliati et al. implied this mechanism as a cause for the presence of $C_{12}H_8^+$ in their plasma [38]. It is plausible that the presence of neutral hydrogen in the plasma may lead to the formation of ions heavier than the molecular ion also in an electric thruster.

## Performance, accommodation, and impact of AHs as EP propellants

### Performance predictions for AHs

Fluorobenzene has a relatively low molecular mass of 96.1 amu, high vapor pressure and low melting point, which could lead to low heater power requirements and higher specific impulse. It could be an attractive candidate for, e.g., power- and volume-constrained satellites, or long-range missions with low available power and high delta-v requirements. The naphthalenes are heavier and therefore better suited for high thrust applications. The larger ionization cross section and lower IE of the AHs compared to that of xenon could result in a comparable or even higher ionization efficiency compared to that of xenon despite ionization-induced fragmentation of the AHs. To put it in perspective, the difference in IE between naphthalene and xenon is 4 eV which translates to about 386 kJ $mol^{-1}$ or 92.2 kcal $mol^{-1}$ (1 mol is approximately 0.13 kg in this case). With an assumed propellant feed rate of 10 mg $s^{-1}$ to the thruster (and disregarding any energy costs associated with fragmentation), the 4 eV difference would equate to a 30-W reduction in power required for total ionization. Furthermore, the mass of naphthalene (128.2 amu) is very close to that of xenon (131.3 amu), making it an ideal benchmark propellant for future testing.

Fragmentation and other plasma processes are expected to negatively impact the ionization efficiency of molecular propellants. Besides ionization induced fragmentation, electron-ion recombination is the process most likely to reduce thruster performance, as recombination reactions between cations and electrons are generally orders of magnitude faster than reactions between ions and neutral molecules [43]. The electron/ion recombination is often referred to as dissociative electron-ion recombination (DR), but the degree of dissociation is difficult to determine experimentally and in the case of aromatic hydrocarbons it is predicted to be low [44, 45]; according to Le Page et al. the recombination leads to an excitation-relaxation process analogous to that of UV absorption, which is

non-dissociative for most AHs [46]. The most probable dissociative process is hydrogen abstraction but there is no experimental evidence for the significance of this mechanism [46]. The DR rate constant has been determined to 3 $10^{-7}$ $cm^3$ $s^{-1}$ [44] and 9 $10^{-7}$ $cm^3$ $s^{-1}$ [45] in independent measurements. The rate constant generally decreases with increasing temperature and for smaller hydrocarbons a temperature dependence of approximately $T^{-1.5}$ has been estimated for temperatures above 300 K [47]. These observations refer to thermal conditions where $T_e = T_+ = T$. It has further been argued that DR may be inhibited by the high electron temperatures in some discharge plasmas [43]. On the basis of available data it is difficult to make a numerical estimate of the effect of DR on the performance of the AH propellants under realistic thruster conditions, but it cannot be excluded that DR may have a significant degrading effect on the performance.

Another process that potentially could reduce the ionization efficiency of molecular propellants is electron impact fluorescence. In this process the molecule is excited to a neutral excited state by electron impact followed by relaxation to the neutral ground state through internal conversion and fluorescence [48, 49]. For naphthalene the cross-section of this process in the temperature range of 0-300 eV has been determined experimentally [49]. The cross-section has an onset at 4.7 eV and rises rather rapidly to a maximum of 0.10 $10^{-20}$ $m^2$ at 6.7 eV followed by a second maximum of 0.11 $10^{-20}$ $m^2$ at 7.8 eV after which it decreases slowly to 0.4 $10^{-20}$ $m^2$ at 70 eV. In comparison, the cross-section for ionization is an order of magnitude larger already at 10 eV and continues to increase rapidly until its maximum at around 60 eV, see Fig. 2. We expect a similar relation between the two types of cross-sections for the fluorinated AHs. Thus, electron impact fluorescence is expected to have a minor influence on the ionization efficiency of the AHs. This is further accentuated by the fact that the process does not lead to any significant fragmentation of naphthalene below 30 eV [48].

Electron attachment is another process that potentially could influence the thruster performance. It has been inferred as one of the major reasons behind the poor performance of $C_{60}$ as propellant for electric propulsion [18–20]. However, in contrast to $C_{60}$, which has an electron affinity of 2.68 eV, all the AHs investigated in this study have a negative electron affinity [50]. Thus, the negative ion is not stable, but exists as a transient species and the electron is expelled shortly after absorption. In fact, the maxima at 6.7 and 7.8 eV in the electron impact fluorescence cross section of naphthalene are resonant excitations, which involve the formation of a temporary negative ion state that decays by electron autodetachment, leaving the neutral molecule in an excited electronic state [49]. Considering the relatively low cross section for forming these resonances compared to the ionization cross section, they are expected to be of low significance for the ionization efficiency. Le Page have also argued that AH anions are much less common than neutrals and cations in plasmas [46]. It should be noted, though, that Alliati et al. report a negative ion mass spectrum for the 15 W microwave pulsed discharge experiment. In this spectrum, the largest peak corresponds to $C_4H^-$ [38]. They argue that this species is most likely formed in a top down process starting from the fragmentation of naphthalene cation. Although electron attachment cannot be entirely ruled out from influencing the thruster performance, it is not expected to be of any greater importance.

We have also considered the relative importance of double excitation for the ionization efficiency of the AHs, as it is known to reduce the efficiency of xenon propelled thrusters. First, we note that for the AHs the second (double) ionization energy is more

than twice higher than the first ionization energy, e.g. for naphthalene they are 19.3 eV and 8.14 eV, respectively [51]. This is in contrast to xenon, which has a second ionization energy (21.0 eV) that is less than 9 eV higher than the first (12.13 eV) [52]. Furthermore, as already has been mentioned, the prominent peak at 64 m/z in the 1000 eV EI-MS spectrum of naphthalene, which has been attributed to double ionization, is essentially absent in our 70 eV spectrum [52]. The 64 m/z peak has low intensity also in the spectrum of Alliati et al., whereas the larger 63 m/z peak is attributed to $C_5H_3^+$ [38]. Similarly as for naphthalene, we note in the EI-MS spectra of the fluorinated AHs that the m/z value corresponding to the doubly ionized molecule has a very low intensity. Thus, the AHs are not expected to be affected by reduced propulsion efficiency due to double ionization to the same extent as xenon.

It should also be noted that molecular propellants differ from atomic propellants in that the molecular ion directly after ionization may end up in a state that is both electronically and vibrationally excited. However, this extra deposition of vibrational energy upon ionization is included in the BEB-calculation as it based upon vertical ionization potentials. Therefore the effect of vibrational excitation upon the ionization efficiency is considered in the energy deposition curves of Fig. 3. After the ionization process the molecular ion transitions to its electronic ground state whereupon the excess electronic energy is converted to vibrational energy in a process called internal conversion, i.e. excitation energy is converted to thermal energy. It is during the internal conversion the molecular ion can dissociate into an ion and a neutral fragment.

#### Propellant storage and delivery

In Table 1 of Appendix A the boiling point and density of several AHs are listed. The density of the AHs in Fig. 1 ranges between 1020 and 1140 kg $m^{-3}$ and the boiling point is in all cases high enough to ensure that they all remain non-gaseous at room temperature and under atmospheric pressure (i.e., at NTP). A propellant stored onboard a satellite can be kept close to NTP, and as the melting point of 1-fluoronaphthalene and fluorobenzene are negative on the Celsius scale, they will remain liquid. Naphthalene is solid at NTP, but the vapor pressure, ~49 Pa at 314 K corresponding to ~10 mg $cm^{-2}$ $s^{-1}$ as per Fig. 6, is sufficient to facilitate the transfer rate required to feed a mN-class thruster and the melting point of 353.4 K is sufficiently high to avoid a solid-liquid phase transition. Vapor pressure data for the fluoronaphthalenes was not available, but the fluoronaphthalenes are assumed to have similar vapor pressure curves as naphthalene, since benzene and the fluorobenzenes have similar vapor pressure curves (also shown in Fig. 6). The vapor pressure of benzene and fluorobenzene at 314 K is 25 and 20 kPa, respectively. For comparison, the vapor pressure of molecular iodine is 144 Pa at 314 K.

While the AHs cannot be compressed to the density of pressurized gaseous propellants like xenon at 186 bar, or the density of heavier atomic propellants like iodine or mercury, they do avoid the added mass and safety considerations of the high-pressure propellant storage equipment required by the former and many material incompatibilities of the latter.

#### Accommodation in electrostatic EP thrusters

Positively charged propellant electrostatically expelled from the thruster must be neutralized to prevent the accumulation of negative charge in the spacecraft. This is

achieved by electron emission, which in addition to neutralizing the exhaust, also feeds electrons for the ionizing plasma. For high power thrusters where high electron currents are needed, neutralization is typically accomplished by thermionic emission in the form of a hollow cathode placed close to the thruster exhaust. This type of cathode needs to be fed with a significant amount of propellant to facilitate the outgoing flow of electron current, all while the actively emitting thermionic material is kept at temperatures normally between 1300 and 2000 °C. At those temperatures most types of molecules will completely disintegrate into their highly reactive atomic constituents. The materials commonly used for thermionic emission are typically fed with very pure and inert xenon, and the performance is very sensitive to changes in their surface chemical composition. Extensive exploration of the literature strongly indicates that hydrocarbons are not compatible with most common types of thermionic emitter materials [53–60]. While research on the poisoning behavior of most emitters is scarce, emitters are likely to be inoperable in non-inert atmospheres because of their fragile and easily disrupted emission capacities.

Alternative electron emission technologies, such as field emission (FE) array cathodes, exist. FE cathodes require no propellant feed or dedicated heating to operate, but they instead rely on a strong electric field to pull electrons from the surface of the material. The achievable emission output is typically limited to only a few mA $cm^{-2}$, whereas high-performance hollow cathodes can be made to emit tens to hundreds of amperes. Recent advances have been made in operating resistant FE array cathodes based on carbon nanotubes in the hazardous environment of Low Earth Orbit, as part of the KITE mission conducted by the Japanese space agency JAXA [61, 62]. Their achieved current output was quite limited, but other researchers have demonstrated optimized CNT array emitters reaching close to 1 A $cm^{-2}$ [63]. In the future, FE cathodes like these could become viable for use with thrusters operated on alternative propellants like the AHs suggested here.

#### Safety Considerations and Environmental Impact

AHs have been linked to several kinds of adverse health effects in humans, both acute and chronic [64], but studies have shown that the toxicity of unsubstituted AHs generally decreases with molecular weight, except for the highly carcinogenic benzene [65]. Naphthalene is classified as harmful if swallowed and suspected to be cancerogenic according to the European Chemicals Agency (ECHA) [66]. The ECHA classification for 1-fluoronaphthalene only states that it causes serious eye irritation, causes skin irritation and may cause respiratory irritation [67]. Fluorobenzene is only classified to cause serious eye damage, although it has been identified that it may cause damage to organs through prolonged or repeated exposure [68]. Naphthalene is very toxic to aquatic life with long-lasting effects. The corresponding effects are less severe for fluorobenzene and 1fluoronaphthalene as indicated by their ECHA classifications [66–68]. It would be necessary to implement appropriate safety procedures for the handling of AHs by ground facility personnel. However, it should be noted that the potential health hazards of the AHs are much less severe than for the highly toxic and carcinogenic monopropellant hydrazine and therefore the safety precautions for AHs would be much less restrictive. In addition, the AHs are not classified as explosives, and handling procedures would be simplified compared to those for monopropellants or xenon under high pressure.

As for potential environmental impact, whereas halogenated hydrocarbons of the heavier halogens may have a damaging effect on the ozone layer when introduced into the stratosphere, it is known that atmospheric fluorine does not lead to depletion of ozone [69]. Fluorocarbons (such as the fluorinated compounds of this study) can contribute to global warming, mainly by absorbing 1000–1400 $cm^{-1}$ IR radiation where the atmosphere is otherwise relatively transparent [70]. It should be noted that the lifetime of the AHs in this study is expected to be relatively short at altitudes above the stratosphere due to high levels of UV-radiation. Thus, the AHs are not likely to contribute to global warming.

## Conclusions

We have evaluated the aromatic hydrocarbon (AH) molecules fluorobenzene ($C_6H_5F$), naphthalene ($C_{10}H_8$), and 1-fluoronaphthalene ($C_{10}H_7F$) for use as alternative propellants in electric propulsion thrusters for in-space propulsion by comparing environmental and safety aspects, material compatibility, storability, cost and predicted ionization efficiency.

Neither naphthalene nor the fluorinated AHs pose a risk of depleting the ozone layer if they were to reach the stratosphere. While appropriate safety procedures would have to be implemented for the handling of AHs, they are not classed as explosives and do not require the safety precautions associated with high-pressure gas and monopropellants.

A literature survey indicates that AHs are incompatible with available emitter materials used in high-current hollow cathode neutralizers, limiting the propellant flow rates and thrust achievable with AH propellants in electrostatic thrusters; however no material compatibility issues are foreseen for cathodeless electromagnetic thrusters.

The AHs are liquid or solid at common satellite propulsion subsystem pressures and temperatures, and while their density is lower compared to high-pressure xenon or propellants like iodine and mercury, they do avoid the added mass and safety considerations of the high-pressure propellant storage equipment required by the former and many material incompatibilities of the latter. The solid/liquid-vapor phase transition properties of the AHs show that they will be compatible with a low-power sublimation-based propellant feed system.

Ionization efficiency was estimated by calculation of the ionization cross section and measurement of the ionization-induced fragmentation. Quantum chemical calculations and Binary Encounter Bethe (BEB) theory were used to calculate the ionization cross section of these AHs. The calculated ionization cross sections for the naphthalenes are more than five times higher than that of xenon. BEB calculations further indicate that 25 eV electrons and electrons from a 7 eV Maxwellian plasma deposit similar amounts of energy into the molecules, allowing estimation of the fragmentation behavior of the molecules in a 7 eV plasma thruster using 25 eV EI-MS. These measurements for the AHs show very low fragmentation with 81–86% of the observed ions originating from intact molecules, compared with 34% for adamantane. Considering that the ionization energy of the AHs is 4 eV lower than that of xenon, the higher ionization cross section together with the low degree of post-ionization dissociation indicate that the ionization efficiency of the AHs could be similar to or greater than that of xenon.

The investigated AHs are considered viable candidates as an alternative propellant to xenon due to their similar mass, lower storage pressure, lower cost, and potentially comparable or higher ionization efficiency.

## 1. APPENDIX A (TABLES AND FIGURES)

**Table 1** Aromatic hydrocarbons (AH) identified as potential EV propellant candidates together with relevant physical properties reported at standard conditions. Adamantane and xenon are included at the bottom for easy comparison. $M_w$=molecular weight, $T_M$=melting point, $T_V$=boiling point, ρ = density, $IE_a$ is the adiabatic ionization energy, and T(ṁ) the temperature corresponding to an estimated evaporation/sublimation rate of ~10 mg $cm^{-2}$ $s^{-1}$ into vacuum as calculated with Eqs. 1 and 2 (Appendix B) using Antoine constants found in Table 3

| | Chemical formula | $M_w$ g $mol^{-1}$ | $T_M$ ($T_V$) °C | ρ kg $m^{-3}$ | 1st $IE_a$ eV | T(ṁ) °C | Bulk price[4] € $kg^{-1}$ |
|---|---|---|---|---|---|---|---|
| benzene | $C_6H_6$ | 78.1 | 5.5 (80.1) | 876 | 9.24 | -57[5] | 38.9 (100 L) |
| fluorobenzene | $C_6H_5F$ | 96.1 | -42 (85) | 1020 | 9.20 | -57[5] | 39.4 (200 kg) |
| cyanobenzene | $C_6H_5CN$ | 103.1 | -10 (191) | 1000 | 9.73 | 11[5] | 47.9 |
| naphthalene | $C_{10}H_8$ | 128.2 | 86.3 (217) | 1140 | 8.14 | 41 | 46.8 |
| 1-fluoronaphthalene | $C_{10}H_7F$ | 146.2 | -13 (215.2) | 1132 | 8.15 | | 93.3 |
| 2-fluoronaphthalene | $C_{10}H_7F$ | 146.2 | 58 (211.6) | 1240 | 8.23 | | |
| fluorene[1] | $C_{13}H_{10}$ | 166.2 | 116 (298) | 1200 | 7.91 | 86 | 73.8 (> 98%) |
| phenanthrene | $C_{14}H_{10}$ | 178.3 | 101 (332) | 1180 | 7.89 | 102 | 147.4 |
| anthracene | $C_{14}H_{10}$ | 178.3 | 216.4 (341) | 1250 | 7.44 | 136 | 83.1 |
| hexafluorobenzene | $C_6F_6$ | 186.1 | 5.2 (80.2) | 1610 | 9.90 | -57[5] | 333.7 |
| pyrene | $C_{16}H_{10}$ | 202.3 | 146 (404) | 1270 | 7.43 | 142[5] | 112.1 (> 98%) |
| anthanthrene[2] | $C_{22}H_{12}$ | 276.3 | 261 (556) | 1377 | 6.92 | 250[5] | |
| coronene | $C_{24}H_{12}$ | 300.3 | 437.3 (525) | 1371 | 7.29 | 309[5] | 12984.6 (> 95%) |
| adamantane | $C_{10}H_{16}$ | 136.2 | 279 | 1080 | 9.25 | | |
| xenon | Xe | 131.3 | -111.8 (-108) | > 1500[3] | 12.13 | | > 2000 |

[1] Not fully aromatic but often considered an AH [2]Commonly referred to as Dibenzo[def,mno]chrysene [3]Storage density can be increased through pressurization [4]Prices obtained in the middle of June 2021 and correspond to order size of 100 kg and ≥ 99% purity unless otherwise stated (estimates produced by Chemtronica AB, www.chemtronica.com/en) [5]Temperature estimated by extrapolation outside the valid range defined for the Antoine constants

**Table 2** Relative ion intensities for the spectra shown in Fig. 4 together with relative ionization cross sections calculated using Binary Encounter Bethe theory

| | T (eV) | $I^T_{M^+}/I^{70}_{M^+}$ | $I_{M^+}/I_{tot}$ | $I_{\sum[M-H_x]^+}/I_{tot}$ | $I^T_{tot}/I^{70}_{tot}$ | $\sigma^T_{BEB}/\sigma^{70}_{BEB}$ |
|---|---|---|---|---|---|---|
| naphthalene | 25 | 0.874 | 0.853 | 0.925 | 0.490 | 0.583 |
| | 40 | 0.958 | 0.567 | 0.673 | 0.809 | 0.879 |
| | 70 | 1.000 | 0.478 | 0.559 | 1.000 | 1.000 |
| 1-fluoronaphthalene | 25 | 0.814 | 0.858 | 0.897 | 0.451 | 0.550 |
| | 40 | 0.911 | 0.578 | 0.642 | 0.747 | 0.857 |
| | 70 | 1.000 | 0.474 | 0.523 | 1.000 | 1.000 |
| fluorobenzene | 25 | 0.769 | 0.808 | 0.844 | 0.467 | 0.523 |
| | 40 | 0.943 | 0.559 | 0.608 | 0.827 | 0.841 |
| | 70 | 1.000 | 0.490 | 0.537 | 1.000 | 1.000 |
| adamantane | 25 | 0.974 | 0.339 | 0.413 | 0.489 | 0.569 |
| | 40 | 1.066 | 0.212 | 0.263 | 0.854 | 0.877 |
| | 70 | 1.000 | 0.170 | 0.212 | 1.000 | 1.000 |

**Table 3** Antoine constants for AHs and benzene analogues and the temperature ranges over which they are defined. No data for 1fluoronaphthalene could be found in the literature

| | Temperature range (K) (°C) | | A | B (K) | C (K) |
|---|---|---|---|---|---|
| Benzene[1] | 280–374 | 7-101 | 5.98523 | 1184.236 | -55.623 |
| Fluorobenzene[2] | 255–357 | -18-84 | 4.36225 | 1409.848 | -34.792 |
| Cyanobenzene[2] | 301–464 | 28–191 | 4.85410 | 2110.572 | -28.331 |
| Naphthalene[1] | 310–353<br>368–523 | 37-80<br>95-250 | 8.70592<br>6.13555 | 2619.91<br>1733.71 | -52.5<br>-71.291 |
| Fluorene[1] | 307–348<br>348–388 | 34-75<br>75-115 | 5.33196<br>8.91036 | 1547.377<br>3245.362 | -133.083<br>-45.893 |
| Phenanthrene[1] | 306-321<br>356-650 | 33-48<br>83-377 | 11.631<br>6.37081 | 4873.4<br>2329.54 | 0.05<br>-77.87 |
| Anthracene[1] | 299–430 | 26–157 | 10.5899 | 4903.3 | -1.58 |
| Hexafluorobenzene[2] | 278–378 | 5-105 | 4.16054 | 1229.449 | -57.503 |
| Pyrene[1] | 298–401 | 25–128 | 10.7545 | 5072.78 | 0.0 |
| Anthanthrene[1] | 465–495 | 192–222 | 12.014 | 7060 | 0.0 |
| Coronene[1] | 430–560 | 157–287 | 8.80062 | 5491.689 | -48.484 |

Pressure given in [1] kPa [71] [2]$10^2$ kPa [50]

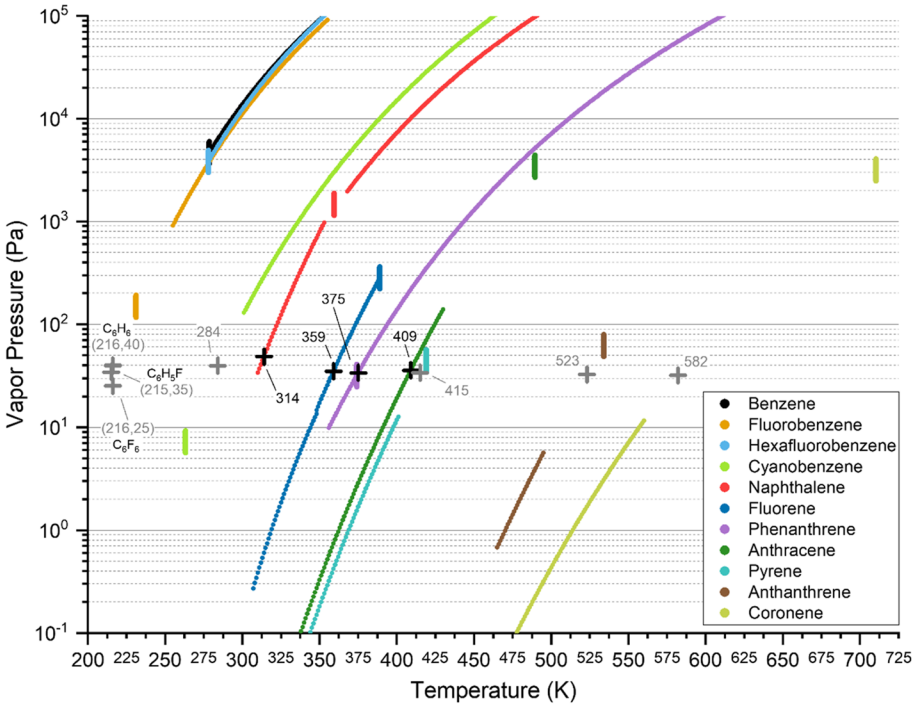


**Fig. 6** Vapor pressures of examined cyclic aromatic hydrocarbons as a function of temperature obtained using data in Table 3 and Eq. 1. The melting point (measured at 25 °C and 100 kPa) for each compound is indicated by vertical lines and the points corresponding to an evaporation mass flow rate of ~ 10 mg $cm^{-2}$ $s^{-1}$ as calculated using Eq. 2 (where $\alpha = 1$ and $P_c = 0$) are marked with a black cross if they are within their respective Antoine temperature range, or a grey cross if they are based on extrapolation outside the range of the source data. These temperatures (and vapor pressures for benzene and the fluorobenzenes) are indicated numerically in the figure

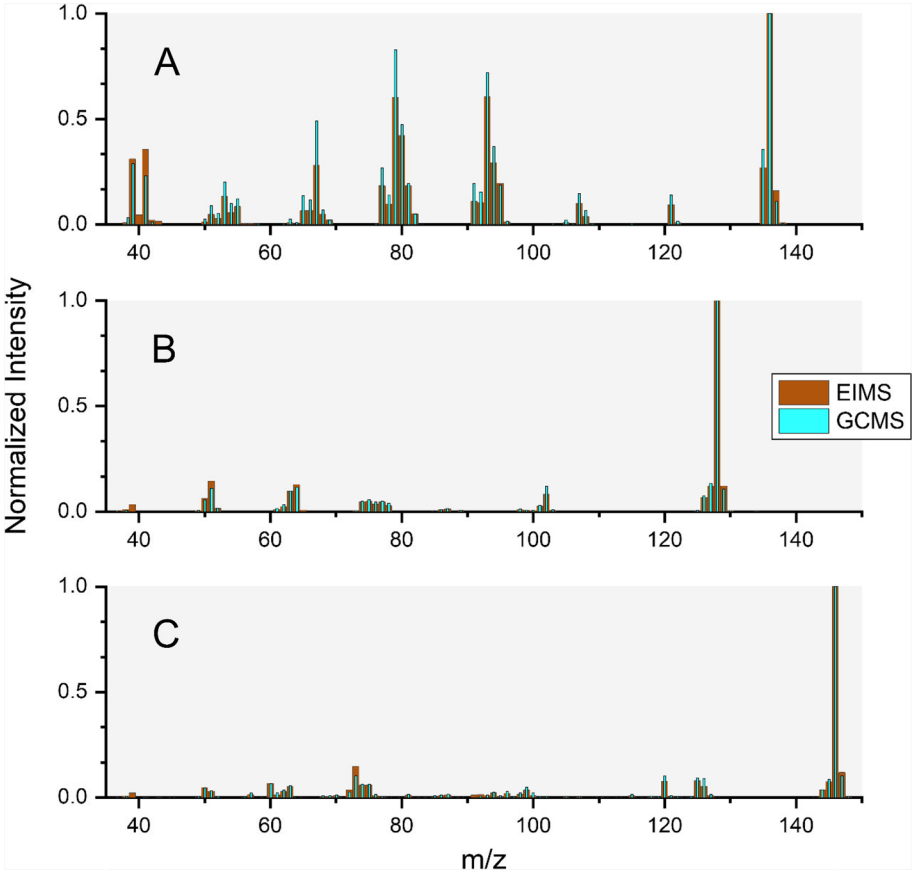


**Fig. 7** Mass spectra of adamantane (A) naphthalene (B) 1-fluoronaphthalene (C), collected by electron ionization mass spectrometry (EI-MS) and gas chromatography mass spectrometry (GCMS) using $T = 70$ eV incident electron kinetic energy. A lower detection limit of m/z = 39 amu was present for the GCMS measurements, therefore the figure above does not include any of the fragments detected with EI-MS below that point

## 2. APPENDIX B (EQUATIONS)

**Eqs. 1–2** Relations for calculating vapor pressures and mass flows by sublimation/evaporation from solid/liquid phase

$$\log_{10}(P_v) = A - \frac{B}{T_s + C} \tag{1}$$

$$\dot{m} = \frac{\alpha A_s (P_v - P_c)}{\sqrt{2\pi k_b T_s m_p^{-1}}} \tag{2}$$

where $A$, $B$, $C$ are Antoine constants, $\dot{m}'$ is the mass flow rate (kg m$^{-2}$s$^{-1}$), $P_v$ and $P_c$ is the respective vapor pressure and surrounding gas pressure (Pa), $k_b$ is the Boltzmann constant, $T_s$ is the surface temperature (K), $m_p$ is the molecular mass (kg), $A_s$ is the surface area (m$^2$) and $\alpha$ is a sticking coefficient.

Equation 3 Binary Encounter Bethe theory [28, 29] used for calculating absolute single-collision (e,2e) ionization cross sections by taking the sum over all (occupied) orbitals $i$ of the target atom or molecule

$$\sigma_{BEB} = \sum_i \sigma_i = \sum_i \frac{4\pi a_0^2 N (R/B_i)^2}{t+u+1}\left[\frac{\ln t}{2}\left(1-\frac{1}{t^2}\right)+1-\frac{1}{t}-\frac{\ln t}{t+1}\right] \tag{3}$$

where $N$ is the orbital occupancy number, $R$ the Rydberg constant, $a_0$ the Bohr radius, $B_i$ the negative orbital binding energy (i.e., the vertical ionization energy to afford a specific electronic state), $U_i$ the orbital kinetic energy, $T$ the kinetic energy of the incident electron, and $u = U/B$ and $t = T/B$ are the reduced versions of $U$ and $T$, respectively. The procedure for calculating $B$ and $U$ is detailed in the method section of this article. Note that $\sigma_i = 0$ if $T < B$ as there is not enough energy to eject an electron from the orbital.

Equation 4 Probability distribution for the energy deposition $E$ into a target molecule or atom resulting from *successful* electron ionization through the (e,2e) process, as presented in the paper by K. Irikura [72]

$$P(E,T) = \frac{\sum_i \delta(E-B_i)\sigma_i(T)}{\sum_i \sigma_i(T)} \tag{4}$$

where $B_i$ and $\sigma_i$ are defined in Eq. 3, $E$ is the energy deposited into the ionization target, and $\delta$ is the Dirac delta function defined by $\delta(x) = 1$ when $x = 0$ and $\delta(x) = 0$ when $x \neq 0$.

Equation 5 Modified version of Eq. 4 used to estimate the probabilistic energy deposition caused by (e,2e) ionization by electrons with energies following a Maxwellian distribution $P_{MB}$

$$P(E,T) = \frac{\sum_i \delta(E-B_i)P_{MB}(T)\sigma_i(T)}{\sum_i P_{MB}(T)\sigma_i(T)} \tag{5}$$

Equation 6 Probabilistic Maxwell-Boltzmann energy distribution derived for massive, non-relativistic particles

$$P_{MB}(T) = 2\left(\frac{T}{\pi T_e^3}\right)^{\frac{1}{2}} exp\left(\frac{-T}{T_e}\right) \tag{6}$$

where $T_e$ is the electron temperature (in eV), and $T$ is (same as Eqs. 3–5) the electron kinetic energy.

Equation 7 Gaussian smoothing function

$$G = \exp(\left(\frac{E-B_i}{\rho}\right)^2 \tag{7}$$

where $\rho = 1.5$ eV is the variance used for all calculations presented in this work, and $E$ and $B_i$ are defined in Eqs. 3 and 4, respectively.

**Acknowledgements**
Special thanks to Dr. Abdusalam Uheida of the KTH Functional Materials Division for allowing us access to his lab and equipment, saving us precious time during the early measurements. Technical assistance by Lea Hohmann at KTH Dep. of Chemical Engineering is gratefully acknowledged.

**Author contributions**
André Nyberg Borrfors (ANB), Simone Ciaralli, Ashley Hallock and Tore Brinck (TB) contributed to the study conception and general design. ANB, Daniel J. Harding and Jonas Weissenrieder contributed to the experimental design and data acquisition. ANB and TB devised the theoretical procedure. ANB performed all computations and analysis of experimental data. ANB wrote the first draft. All authors commented on previous versions of the manuscript, read and approved the final manuscript.

**Funding**
Open access funding provided by Royal Institute of Technology. This work was initiated by OHB Sweden through the NFRP 4 program and is supported by the Swedish National Space Agency. Additional funding to DJH was provided by the Swedish Foundation for Strategic Research (SSF) (ITM17-0236). Additional funding to JW was provided by the Swedish Research Council (VR) (2021–87883).

**Conflict of interest**
The authors have no competing interests to declare that are relevant to the content of this article.

**Data Availability**
Computational and experimental data are available from the corresponding author upon reasonable request.

**Code Availability**
Not applicable.

## Declarations

**Competing interests**
The authors declare no competing interests.

Received: 7 March 2023 Accepted: 28 September 2023
Published online: 16 November 2023

**References**

1. Kieckhafer A, King LB (2007) Energetics of propellant options for high-power Hall thrusters. J Propul Power 23:21–26. https://doi.org/10.2514/1.16376
2. Szabo J, Robin M, Duggan J, Hofer RR (2009) Light metal propellant Hall thrusters. 31st International Electric Propulsion Conference (IEPC-138) 1–12
3. Szabo J, Robin M, Paintal S, Pote B, Hruby V (2012) High density Hall thruster propellant investigations. 48th AIAA/ASME/SAE/ASEE Joint Propulsion Conference and Exhibit 2012 1–15. https://doi.org/10.2514/6.2012-3853
4. Szabo J, Robin M, Hruby V (2017) Bismuth vapor Hall effect thruster performance and plume experiments. 35th International Electric Propulsion Conference (IEPC-25) (October 2017):1–13
5. Doyle KP, Peck MA (2019) Water electrolysis propulsion as a case study in resource-based spacecraft architecture (February 2020). IEEE Aero El Sys Mag 34:4–19. https://doi.org/10.1109/MAES.2019.2923312
6. Schwertheim A, Knoll A (2021) Low power thrust measurements of the water electrolysis Hall effect thruster. CEAS Space J 14:3–17. https://doi.org/10.1007/s12567-021-00350-y
7. Branam R (2016) AFRL-AFOSR-VA-TR-2016-0381 iodine plasma (electric propulsion) interaction with spacecraft materials, Technical Report. University of Alabama, https://apps.dtic.mil/sti/pdfs/AD1023812.pdf
8. Dankanich JW, Szabo J, Pote B, Oleson S, Kamhawi H (2014) Mission and system advantages of iodine Hall thrusters. 50th AIAA/ASME/SAE/ASEE Joint Propulsion Conference 1–11. https://doi.org/10.2514/6.2014-3905
9. Hua Z, Wang P, Ning Z, Ye Z, Xu Z (2022) Early experimental investigation of the C12A7 hollow cathode fed on iodine. Plasma Sci Technol. https://doi.org/10.1088/2058-6272/ac4fb4
10. Rafalskyi D, Martínez JM, Habl L, Zorzoli Rossi E, Proynov P, Boré A, Baret T, Poyet A, Lafleur T, Dudin S, Aanesland A (2021) In-orbit demonstration of an iodine electric propulsion system. Nature 599:411–415. https://doi.org/10.1038/s41586-021-04015-y
11. Szabo J, Pote B, Paintal S, Robin M, Kolencik G, Hillier A, Branam RD, Huffman RE (2011) Performance evaluation of an iodine vapor Hall thruster. 47th AIAA/ASME/SAE/ASEE Joint Propulsion Conference and Exhibit 1–20. https://doi.org/10.2514/1.58835
12. Taillefer ZR, Blandino JJ, Szabo J (2020) Characterization of a barium oxide cathode operating on xenon and iodine propellants. J Propul Power 36(4):575–585
13. Thompson SJ, Vangemert JJ, Farnell CC, Farnell CC, Farnell SC, Hensen TJ, Ham RK, Williams DD, Chandler JP, Williams JD (2019) Development of an iodine compatible hollow cathode. AIAA Propulsion and Energy Forum (AIAA-2019-3997. 1–7. https://doi.org/10.2514/6.2019-3997
14. Dietz P, Holste K, Gartner W, Kohler PE, Klar PJ, Schreiner PR (2017) Status report of diamondoids as alternative propellants for ion-thrusters. The 35th International Electric Propulsion Conference (IEPC-198)
15. Dietz P, Gartner W, Koch Q, Kohler PE, Teng Y, Schreiner PR, Holste K, Klar PJ (2019) Molecular propellants for ion thrusters. Plasma Sources Sci T 28:84001. https://doi.org/10.1088/1361-6595/ab2c6c

16. Holste K, Dietz P, Scharmann S, Keil K, Henning T, Zschätzsch D et al (2020) Ion thrusters for electric propulsion: scientific issues developing a niche technology into a game changer. Rev Sci Instrum. https://doi.org/10.1063/5.0010134
17. Mansoori GA (2007) Diamondoid molecules. Adv Chem Phys 136:207–258
18. Leifer SD, Rapp D, Saunders WA (1992) Electrostatic propulsion using $C_{60}$ molecules. J Propul Power 8:1297–1300. https://doi.org/10.2514/3.11476
19. Scharlemann CA (2002) Theoretical and experimental investigation of $C_{60}$-propellant for ion propulsion. Acta Astronaut 51:865–872. https://doi.org/10.1016/S0094-5765(02)00115-7
20. Nakayama Y, Takegahara H (2008) IEPC-95-88 fundamental experiments of $C_{60}$ application to ion thruster. 24th International Electric Propulsion Conference (IEPC)
21. Chen Z, Wu JI, Corminboeuf C, Bohmann J, Lu X, Hirsch A, Schleyer PVR (2012) Is $C_{60}$ buckminsterfullerene aromatic. Phys Chem Chem Phys 14:14886–14891. https://doi.org/10.1039/C2CP42146A
22. Chanyshev AD, Litasov KD, Furukawa Y, Kokh KA, Shatskiy AF (2017) Temperature-induced oligomerization of polycyclic aromatic hydrocarbons at ambient and high pressures. Sci Rep-UK 7:1–8. https://doi.org/10.1038/s41598-017-08529-2
23. Chanyshev AD, Litasov KD, Shatskiy AF, Sharygin IS, Higo Y, Ohtani E (2017) Transition from melting to carbonization of naphthalene, anthracene, pyrene and coronene at high pressure. Phys Earth Planet in 270:29–39. https://doi.org/10.1016/j.pepi.2017.06.011
24. Madison JJ, Roberts RM (1956) Pyrolysis of aromatics and related heterocyclics. ACS Div Petroleum Chem Inc Preprints 1:56–79. https://doi.org/10.1021/ie50578a044
25. Stein SE, Fahr A (1985) High-temperature stabilities of hydrocarbons. J Phys Chem 89:3714–3725. https://doi.org/10.1021/j100263a027
26. Johns IB, McElhill EA, Smith JO (1962) Thermal stability of some organic compounds. J Chem Eng Data 7:277–281. https://doi.org/10.1021/je60013a036
27. Frisch MJ, Trucks GW, Schlegel HB, Scuseria GE, Robb MA, Cheeseman JR et al (2016) Gaussian 16 suite of Programs. Gaussian, Inc., Wallingford
28. Kim Y-K, Rudd ME (1994) Binary-encounter-dipole model for electron-impact ionization. Phys Rev A 50:3954–3967. https://doi.org/10.1103/PhysRevA.50.3954
29. Stone PM, Kim YK (2005) An overview of the BEB method for electron-impact ionization of atoms and molecules. Surf Interface Anal 37(11):966–968
30. Goebel DM, Katz I (2008) Fundamentals of Electric Propulsion: Ion and Hall Thrusters, JPL Space Science and Technology Series, Jet Propulsion Laboratory. California Institute of Technology. https://doi.org/10.1002/9780470436448
31. Rejoub R, Lindsay BG, Stebbings RF (2002) Determination of the absolute partial and total cross sections for electron-impact ionization of the rare gases. Phys Rev A 65:8. https://doi.org/10.1103/PhysRevA.65.042713
32. Wüest M, Evans DS, Von Steiger R (2007) Calibration of Particle Instruments in Space Physics. Appendix H, International Space Science Institute, Bern, Switzerland
33. Ali MA, Kim YK, Hwang W, Weinberger NM, Rudd ME (1997) Electron-impact total ionization cross sections of silicon and germanium hydrides. J Chem Phys 106:9602–9608. https://doi.org/10.1063/1.473842
34. Bart M, Harland PW, Hudson JE, Vallance C (2001) Absolute total electron impact ionization cross-sections for perfluorinated hydrocarbons and small halocarbons. Phys Chem Chem Phys 3:800–806. https://doi.org/10.1039/b009243f
35. Kim YK, Hwang W, Weinberger NM, Ali MA, Rudd ME (1997) Electron-impact ionization cross sections of atmospheric molecules. J Chem Phys 106:1026–1033. https://doi.org/10.1063/1.473186
36. Bull JN, Lee JWL, Vallance C (2014) Absolute electron total ionization cross-sections: molecular analogues of DNA and RNA nucleobase and sugar constituents. Phys Chem Chem Phys 16:10743–10752. https://doi.org/10.1039/c4cp00490f
37. Margolin Eren KJ, Elkabets O, Amirav A (2020) A comparison of electron ionization mass spectra obtained at 70 ev, low electron energies, and with cold ei and their nist library identification probabilities. J Mass Spectrom. https://doi.org/10.1002/jms.4646
38. Alliati M, Donaghy D, Tu X, Bradley JW (2019) Ionic species in a naphthalene plasma: understanding fragmentation patterns and growth of PAHs. J Phys Chem A 123:2107–2113. https://doi.org/10.1021/acs.jpca.9b00100
39. Najeeb PK, Kadhane U (2017) Relative stability of naphthalene, quinoline and isoquinoline under high energy electron impact. Int J Mass Spectrom 414:23–30. https://doi.org/10.1016/j.ijms.2016.12.011
40. Liu X, Shemansky DE (2004) Ionization of molecular hydrogen. Astrophys J 614:1132–1142. https://doi.org/10.1086/423890
41. Schlathölter T, Mostafa Y, Kamman A, Dongelmans A, Arribard Y, Cazaux S et al (2020) Atomic hydrogen interactions with small polycyclic aromatic hydrocarbons cations. Eur Phys J D 74:114. https://doi.org/10.1140/epjd/e2020-10111-y
42. Lemmens AK, Rap DB, Thunnissen JMM, Willemsen B, Rijs AM (2020) Polycyclic aromatic hydrocarbon formation chemistry in a plasma jet revealed by IR-UV action spectroscopy. Nat Commun 11:269. https://doi.org/10.1038/s41467-019-14092-3
43. Smith D, Adams NG (1984) Elementary interactions between charged and neutral species in plasmas. Pure Appl Chem 56:175–188. https://doi.org/10.1351/pac198456020175
44. Biennier L, Alsayed-Ali M, Foutel-Richard A, Novotny O, Carles S, Rebrion-Rowe C, Rowe B (2006) Laboratory measurements of the recombination of pah ions with electrons: implications for the pah charge state in interstellar clouds. Faraday Discuss 133:289–301. https://doi.org/10.1039/B516858A
45. Wiens JP, Shuman NS, Viggiano AA (2015) Dissociative recombination and mutual neutralization of heavier molecular ions: $C_{10}H_8^+$, $WF_5^+$, and $C_nF_m^+$. J Chem Phys 142:114304. https://doi.org/10.1063/1.4913829
46. Le Page V, Snow TP, Bierbaum VM (2001) Hydrogenation and charge states of pahs in diffuse clouds. I. Development of a model. Astrophys J Suppl Ser (ApJS) 132:233. https://doi.org/10.1086/318952

47. McLain JL, Poterya V, Molek CD, Babcock LM, Adams NG (2004) Flowing afterglow studies of the temperature dependencies for dissociative recombination of $O_2^+$, $CH_5^+$, $C_2H_5^+$, and $C_6H_7^+$ with electrons. J Phys Chem A 108:6704–6708. https://doi.org/10.1021/jp040215l
48. Smyth KC, Schiavone JA, Freund RS (2008) Excitation of fluorescence in naphthalene and azulene by electron impact. J Chem Phys 62:136–144. https://doi.org/10.1063/1.430246
49. McConkey JW, Trajmar S, Man KF, Ratliff JM (1992) Excitation of naphthalene by electron impact. J Phys B: at Mol Opt Phys 25:2197. https://doi.org/10.1088/0953-4075/25/9/023
50. Linstrom PJ, Mallard WG (2021) NIST Chemistry WebBook, National Institute of Standards and Technology, Gaithersburg MD, 20899. https://doi.org/10.18434/T4D303
51. Mayer PM, Blanchet V, Joblin C (2011) Threshold photoelectron study of naphthalene, anthracene, pyrene, 1,2-dihydronaphthalene, and 9,10-dihydroanthracene. J Chem Phys 134:244312. https://doi.org/10.1063/1.3604933
52. Haynes WM (2015) CRC Handbook of Chemistry and Physics, 95 edn. CRC Press/Taylor and Francis, Boca Raton, FL
53. Avdienko AA, Malev MD (1977) Poisoning of $LaB_6$ cathodes. Vacuum 27:583–588. https://doi.org/10.1016/S0042-207X(77)80438-7
54. Buckingham JD (1965) Thermionic emission properties of a lanthanum hexaboride/rhenium cathode. Brit J Appl Phys 16:1821–1832. https://doi.org/10.1088/0508-3443/16/12/306
55. Futamoto M, Nakazawa M, Usami K, Hosoki S, Kawabe U (1980) Thermionic emission properties of a single-crystal $LaB_6$ cathode. J Appl Phys 51:3869–3876. https://doi.org/10.1063/1.328132
56. Gallagher HE (1969) Poisoning of $LaB_6$ cathodes. J Appl Phys 40:44–51. https://doi.org/10.1063/1.1657092
57. Nikrant A (2019) Development and Modelling of a Low Current $LaB_6$ Heaterless Hollow Cathode, M.Sc. thesis. Virginia technic Institute and State University, Blacksburg, USA
58. Schmidt KM, Misture ST, Graeve OA, Vasquez VR (2019) Interaction of hydrogen with $MB_6$ (M = Ba, Ca, La, and Sr) surfaces from first principles. ACS Omega 4:65–72. https://doi.org/10.1021/acsomega.8b02652
59. Taran A, Loyan AV, Voronovich D (2007) Comparative high-current-density emitters poisoning of hollow cathodes electric propulsion. 30th International Electric Propulsion Conference (IEPC-270)
60. Yamamoto N, Rokuta E, Hasegawa Y, Nagao T, Trenary M, Oshima C, Otani S (1996) Oxygen adsorption on $LaB_6$ (100) and (111) surfaces. Surf Sci 357–358:708–711. https://doi.org/10.1016/0039-6028(96)00250-6
61. Ohkawa Y, Okumura T, Iki K, Okamoto H, Kawamoto S (2019) Operation of a carbon nanotube field-emission cathode in low earth orbit. J Vac Sci Technol B 37:022203. https://doi.org/10.1116/1.5067299
62. Yamamoto N, Morita T, Ohkawa Y, Nakano M, Funaki I (2019) Ion thruster operation with carbon nanotube field emission cathode. J Propul Power 35:490–493. https://doi.org/10.2514/1.B37214
63. Chouhan V, Noguchi T, Kato S (2016) Field emission from optimized structure of carbon nanotube field emitter array. J Appl Phys 119. https://doi.org/10.1063/1.4945581
64. Abdel-Shafy HI, Mansour MSM (2016) A review on polycyclic aromatic hydrocarbons: source, environmental impact, effect on human health and remediation. Egypt J Petrol 25:107–123. https://doi.org/10.1016/j.ejpe.2015.03.011
65. Geier MC, Chlebowski AC, Truong L, Massey Simonich SL, Anderson KA, Tanguay RL (2018) Comparative developmental toxicity of a comprehensive suite of polycyclic aromatic hydrocarbons. Arch Toxicol 92:571–586. https://doi.org/10.1007/s00204-017-2068-9
66. Brief Profile: Naphthalene, European Chemical Agency (ECHA) – An Agency of European Union, https://echa.europa.eu/brief-profile/-/briefprofile/100.005.717, Acessed 17 Nov 2022
67. Brief Profile: 1-Fluoronaphthalene, European Chemical Agency (ECHA) – An Agency of European Union. https://echa.europa.eu/brief-profile/-/briefprofile/100.005.717. Accessed 17 Nov 2022
68. Brief Profile: Fluorobenzene, European Chemical Agency (ECHA) – An Agency of European Union, https://echa.europa.eu/brief-profile/-/briefprofile/100.006.657, Acessed 17 Nov 2022
69. Ricaud P, Lefévre F (2006) Fluorine in the atmosphere. Fluor Environ 1:1–32. https://doi.org/10.1016/S1872-0358(06)01001-3
70. McCulloch A (2003) Fluorocarbons in the global environment: a review of the important interactions with atmospheric chemistry and physics. J Fluor Chem 123:21–29. https://doi.org/10.1016/S0022-1139(03)00105-2
71. Hall KR, Dykyj J, Svoboda J, Wilhoit RC, Frenkel M (1999) Vapor Pressure of Chemicals - Vapor Pressure and Antoine Constants for Hydrocarbons, and S, Se, Te, and Halogen Containing Organic Compounds, Springer-Verlag, Berlin. https://doi.org/10.1007/b71086
72. Irikura KK (2017) Ab initio computation of energy deposition during electron ionization of molecules. J Phys Chem A 121:7751–7760. https://doi.org/10.1021/acs.jpca.7b07993


## Publisher's Note